Progress In Electromagnetics Research C, Vol. 78, 83–92, 2017

A Miniaturized Microstrip Lowpass Filter with Sharp Skirt Performance and Wide Stopband Utilizing Modified Hairpin Resonator with Long Straight Slots

Ashkan Abdipour*, Alireza Nouritabar, Arash Abdipour, Hossein Shamsi, and Seyed A. Ahmadi

Abstract—In this paper, a lowpass filter with -3 dB cutoff frequency of 1.69 GHz employing modified hairpin resonator with long straight slots is designed. In the first step, to design the primary resonator, the open stubs of a conventional hairpin resonator are folded inside its free area, which results in a smaller occupied area and an improved frequency response. Next, to control the scattering parameters, asymmetric coupled lines with slots are utilized instead of symmetric open-stubs of the primary resonance cell. In each step, the impact of the employed microstrip transmission lines on the scattering parameters of the designed resonator is determined by extracting the equations of the insertion loss (S_{21}) and return loss (S_{11}) on the basis of their equivalent LC circuit. Finally, by using two modified resonators with slots which are placed symmetrically around (Y) axis a sharp transition band (264 dB/GHz) and wide stopband from 1.78 GHz to 10 GHz with a suppressing level of -20 dB are obtained. The overall circuit size is $0.140\lambda_g \times 0.076\lambda_g$, which indicates a small circuit size. The proposed lowpass filter has a high figure of merit equal to 72032.

1. INTRODUCTION

Nowadays, the need of suppressing spurious frequencies to improve the quality of transmitting signals leads to proposing lowpass filters (LPFs) with good in-band and out-band features. For instance, stepped impedance hairpin resonator with radial stubs is employed to design an LPF with wide stopband in [1]. Unfortunately, this circuit does not have a sharp transition band. To design an LPF with wide stopband, a cascaded microstrip coupled-line hairpin unit, semi-circle defected ground structures (DGSs) and semi-circle stepped-impedance shunt stubs are utilized [2]. However, LPFs using DGS structure cannot be used on metal surfaces. In [3], LC resonant structures and transformed radial stubs are employed, and an LPF with an ultra-wide stopband is proposed. However, the circuit occupies a relatively large area. A microstrip lowpass filter featuring compact size and ultra-wide stopband by utilizing both triangular and polygonal patch resonators is designed [4]. In [5], to design an LPF with ultra-wide stopband triangular and radial patch resonators are employed. However, the proposed circuits in [4] and [5] have not been able to provide a sharp transition band and a high level of suppression in the stopband. In addition to the mentioned drawbacks, gradual roll-off rate and low level of relative stopband bandwidth [6–8], narrow stopband bandwidth [9] and also large occupied area [10] have influenced the frequency response of each designed LPF, negatively. Another technique to design an LPF is employing asymmetric high-low impedance patches, which is introduced in [11], but this circuit does not have an acceptable in-band performance. One more approach to design an LPF with sharp transition band is using LC tank resonators, which is reported in [12]. However, this filter occupies a large area. In [13], a lowpass filter

Received 27 July 2017, Accepted 14 September 2017, Scheduled 29 September 2017
* Corresponding author: Ashkan Abdipour (Ashkan_Abdipour@yahoo.com).
The authors are with the Young Researchers and Elite Club, Kermanshah Branch, Islamic Azad University, Kermanshah, Iran.

using polygon patch resonant cells, T-shaped resonators and two different suppressing cells is designed; however, this filter does not have a sharp transition band. Another method to design an LPF with acceptable frequency response is cascading resonators with polygon patches [14], but it has a large circuit size. In [16], coupling stepped-impedance triangular resonators are employed to design an LPF, but it does not have a flat response in the stopband. In this article, a compact lowpass filter using modified hairpin resonance cell with -3 dB cutoff frequency of 1.69 GHz is proposed. In the designed LPF, by employing a pair of the mentioned resonators, a sharp roll-off and a wide stopband are obtained.

2. THE PROCEDURE OF DESIGNING

The configuration and equivalent LC circuit of the conventional hairpin resonator (CHR) with 2 GHz cutoff frequency are illustrated in Figs. 1(a) and 1(b) [17]. The values of lumped elements are as follows: $Cp1 = 1.981$ pF, $Cp2 = 0.285$ pF, $La = 0.091$ nH, $Lb = 3.485$ nH and $Cg = 0.091$ pF. According to the frequency response of CHR, depicted in Fig. 1(c), this filter does not have a wide stopband and sharp roll-off (24.6 dB/GHz). As can be seen from Fig. 1(c), the CHR occupies a large area (3.3 mm$\times$9 mm). To decrease the occupied area and improve the performance, two symmetric coupled lines (SCL) are placed inside the free area of CHR, as shown in Fig. 1(d). This structure decreases the occupied area more than 42% than the CHR. Moreover, the primary modified unit improves the frequency response. According to the illustrated EM simulation result shown in Fig. 1(f), the insertion loss from DC to almost 2 GHz is close to zero, and the transition band is sharpened (85.97 dB/GHz). In addition, the

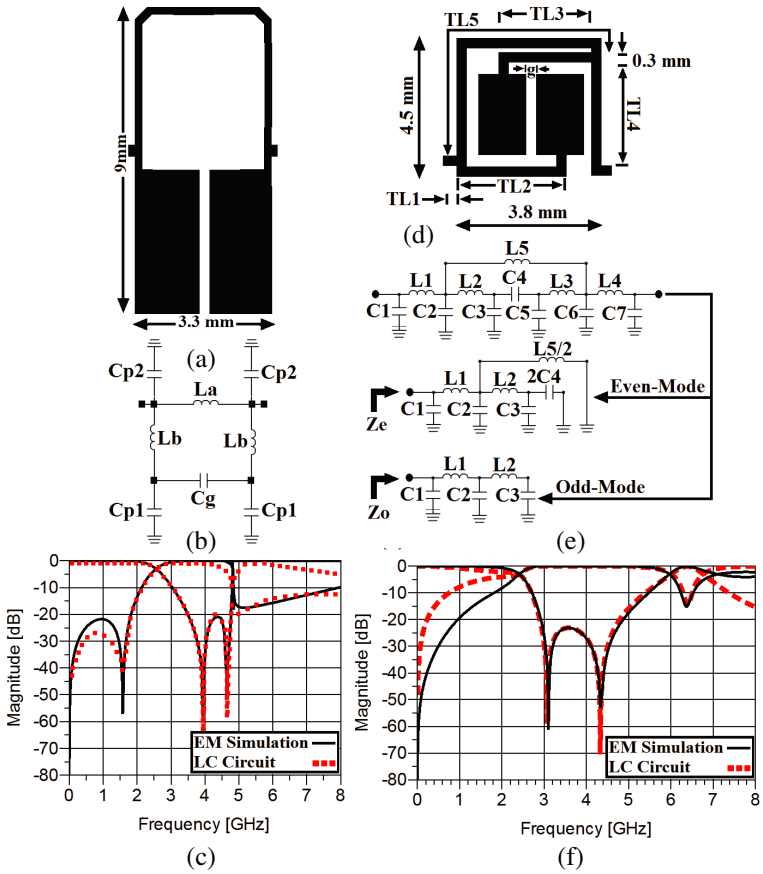

Figure 1. (a) The configuration of the conventional hairpin resonator (CHR) [7]. (b) Its equivalent LC circuit. (c) The result of EM-simulation of CHR. (d) The configuration of the primary symmetric hairpin resonator. (e) Its equivalent LC circuit even-mode and odd-mode excitation. (f) The result of EM-simulation of the primary hairpin resonator.

second transition zero of the conventional circuit located on 4.63 GHz is shifted to higher frequencies leading to widening the stopband region of the main resonator which covers a frequency range from 2.86 up to 4.972 GHz with a suppressing level of −20 dB. Fig. 1(e) illustrates the equivalent LC circuit of the primary modified hairpin resonator. In the depicted lumped circuit, L2, L3, and L5 are equivalent inductors of TL2, TL3, and TL5, respectively. The gap g between two symmetric coupled lines causes a capacitance, which is modeled by C4. Furthermore, C1, C2, C3, C5, C6, and C7 denote the capacitance between the microstrip structure and the ground. L1 and L4 are equivalent inductors of input and output transmission lines (TL1, TL4), respectively. To justify which lump elements of LC circuit, and consequently which corresponding microstrip lines, can control the frequency response, the equations of insertion loss (S_{21}) and return loss (S_{11}) on the basis of the lumped circuit are extracted as follows [16]:

$$S_{21} = \frac{(Z_e - Z_o)\, Z_s}{(Z_e + Z_s)\,(Z_e + Z_s)} \tag{1}$$

$$S_{11} = \frac{Z_o Z_e - Z_s^2}{(Z_e + Z_s)\,(Z_e + Z_s)} \tag{2}$$

Z_s, Z_e and Z_o are source impedance, even- and odd-mode input impedances, respectively. The even- and odd-mode input impedances can be expressed as:

$$Z_o = \frac{1 + (L_1C_2 + L_1C_3 + L_2C_3)\, S^2 + (L_1L_2C_2C_3)S^4}{S\left[(C_1 + C_2 + C_3) + (L_2C_2C_3 + L_1C_1C_3 + L_1C_1C_2 + L_2C_1C_3)\, S^2 + (L_1L_2C_1C_2C_3)S^4\right]} \tag{3}$$

$$Z_e = \frac{S\left[(L_1 + L_5) + (L_2L_5C_a + L_1L_2C_a + L_1L_5C_2 + L_2C_1C_3 + L_1L_5C_a)\, S^2 + (L_1L_2L_5C_2C_a)S^4\right]}{\begin{pmatrix} 1 + (L_2C_a + L_5C_2 + L_5C_a + L_1C_1 + L_5C_1)\, S^2 + (L_2L_5C_2C_a + L_2L_5C_1C_a + L_1L_2C_1C_a + \\ L_1L_5C_1C_2 + L_1L_5C_1C_a)S^4 + (L_1L_2L_5C_1C_2C_a)S^6 \end{pmatrix}} \tag{4}$$

where $C_a = (C_3 + 2C_4)$.

According to Equation (1), the intersection of $Z_{(\text{even})}$ and $Z_{(\text{odd})}$ leads to obtaining the transmission zeros of the primary resonator in the stopband region which can be given as:

$$fz1 = \frac{\left(L2C3 + L2C4 + C4L3 + C5L3 + C4L5 + \sqrt{(L2C3 + L2C4 + C4L3 + C5L3 + C4L5)^2 - 4L2L3\,(C3C4 + C3C5 + C4C5)} \right)}{4\pi L2L3\,(C3C4 + C3C5 + C4C5)} \tag{5}$$

$$fz2 = \frac{\left(L2C3 + L2C4 + C4L3 + C5L3 + C4L5 - \sqrt{+(L2C3 + L2C4 + C4L3 + C5L3 + C4L5)^2 - 4L2L3\,(C3C4 + C3C5 + C4C5)} \right)}{4\pi L2L3\,(C3C4 + C3C5 + C4C5)} \tag{6}$$

In order to obtain high suppression factor, the calculated input impedances, i.e., $Z_{(\text{even})}$ and $Z_{(\text{odd})}$, have to be close to each other in the rejection band region (see Equation (1)). To approximate $Z_{(\text{even})}$ to $Z_{(\text{odd})}$, the odd-mode input impedance can be kept constant and the even-mode input impedance moved toward $Z_{(\text{odd})}$. According to Equations (3) and (4), to control $Z_{(\text{even})}$ without changing the obtained $Z_{(\text{odd})}$, the coupling capacitance (C4) can be utilized (compare Figs. 1(c) and 1(d)). Moreover, the locations of both transmission zeros, i.e., FZ1 and FZ2 can be controlled by the mentioned capacitance based on Equations (5) and (6). To justify the effects of the coupling capacitance (C4) on the calculated frequency response (Equations (1) and (2)) of the shown resonator in Fig. 1(a), several simulations versus C4 are plotted in Fig. 2. By increasing the value of C4 from 0.025 to 0.185 mm with steps of 0.08, not only the first transition zero (FZ1) at 2.05 GHz will move to lower frequencies causing a sharper transition band, but also the −3 dB cutoff frequency decreases. Furthermore, the second transmission zero moves toward higher frequencies causing a wider rejection band as C4 is increased.

This increase makes the return loss better, but not significantly. Unfortunately, fabrication restriction related to the lowest gap between two microstrip lines will reduce the freedom of using the coupling effects. The values of lumped elements of the illustrated circuit in Fig. 1(e) are as follows: $C1 = C7 = 0.387$ pF, $C2 = C6 = 0.39$ pF, $C3 = C5 = 0.7358$ pF, $C4 = 0.085$ pF, $L1 = L4 = 0.327$ nH, $L2 = L3 = 1.354$ nH and $L5 = 2.385$ nH. According to Equations (5) and (6), to control the frequency response and in particular the location of transmission zeros, the capacitances $C3$ and $C5$ which have

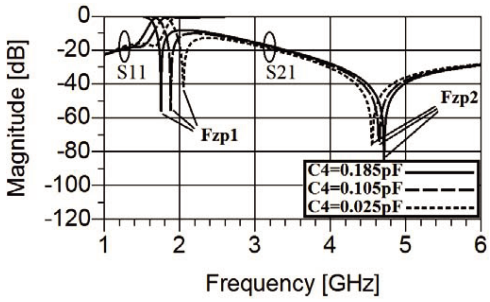

Figure 2. Calculated frequency response with different Cg.

the same capacities and the inductances $L2$ and $L3$ which have the same values can be utilized. It means that the mentioned lumped elements with different values, i.e., $C3 \neq C5$ and $L2 \neq L3$, can be used instead. Thus, to have more degree of freedom in controlling the obtained transmission zeros, microstrip coupled lines with different dimensions can be employed instead of the primary coupled lines with the same dimensions. Clearly, employing coupled lines with different dimensions affects the equivalent LC circuit of the resonator. This asymmetry in open-stubs of the structure of the primary hairpin resonator can be modeled by a capacitance determined by Csp. This capacitance can be calculated as follows [15]:

$$C_{SP} = \varepsilon_0 \varepsilon_r w/h \quad \text{(F/unitLength)} \tag{7}$$

Figure 3 illustrates the designed asymmetric hairpin resonator and its equivalent LC circuit. The above-mentioned capacitance accounts for the microstrip open-stub determined by (B) in Fig. 3(a).

To justify which lump elements of LC circuit, and consequently which corresponding microstrip lines, can control the frequency response, the equations of insertion loss (S_{21}) and return loss (S_{11}) on the basis of the lumped circuit are extracted. To calculate the mentioned equations, the admittance

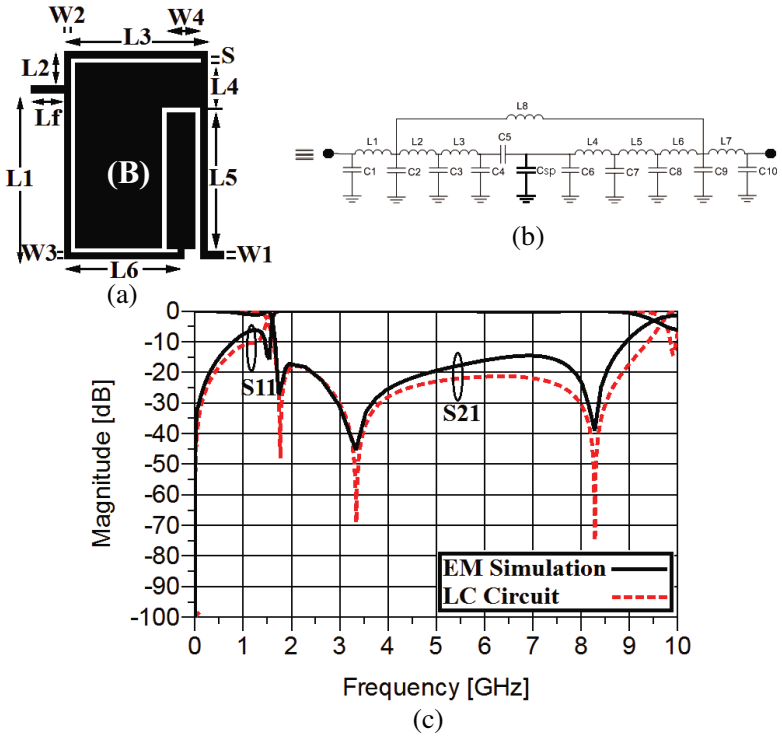

Figure 3. The designed asymmetric hairpin resonator and its equivalent LC circuit.

matrix can be utilized:

$$Y_{\text{Asymmetric Hairpin Resonator}} = \begin{bmatrix} \left(\frac{C}{B}+as+\frac{1}{rs}\right) & -\left(\frac{1}{B}+\frac{1}{rs}\right) \\ -\left(\frac{1}{B}+\frac{1}{rs}\right) & \left(\frac{A}{B}+ps+\frac{1}{rs}\right) \end{bmatrix} \tag{8}$$

Thus, the insertion loss and return loss can be given as follows [15]:

$$S_{21} = \frac{-2Y_{21}Y_o}{\Delta Y} \tag{9}$$

$$S_{11} = \frac{(Y_o-Y_{11})(Y_o+Y_{21})+Y_{21}Y_{12}}{\Delta Y} \tag{10}$$

$$\Delta Y = \frac{E+Fs+ABars^2+B^2raps^3}{B^2rs} \tag{11}$$

$$E = CB+AB-2B \tag{12}$$

$$F = ACr+CBrp+B^2(a+p) \tag{13}$$

where

$$\begin{aligned} A = {} & 1+s^2(hk+hn+mn+hkmns^2+d(e+f+g+k+n+((e+f+g)hk+((e+f+g)h \\ & +(e+f+g+k)m)n)s^2+(e+f+g)hkmns^4)+b(c+e+f+g+k+n+((e+f+g)hk \\ & +((e+f+g)h+(e+f+g+k)m)n+c(hk+(h+m)n+d(e+f+g+k+n)))s^2 \\ & +(cd(e+f+g)hk+(e+f+g)hkmn+c(d(e+f+g)h+hkm+d(e+f+g+k)m)n)s^4 \\ & +cd(e+f+g)hkmns^6)) \end{aligned} \tag{14}$$

$$\begin{aligned} B = {} & s(c+e+f+g+k+n+((e+f+g)hk+((e+f+g)h+(e+f+g+k)m)n+c(hk+(h+m)n \\ & +d(e+f+g+k+n)))s^2+(cd(e+f+g)hk+(e+f+g)hkmn+c(d(e+f+g)h+hkm \\ & +d(e+f+g+k)m)n)s^4+cd(e+f+g)hkmns^6) \end{aligned} \tag{15}$$

$$\begin{aligned} C = {} & 1+cds^2+hs^2(c+e+f+g+cd(e+f+g)s^2)+ms^2(c+e+f+g+k+(cd(e+f+g) \\ & +(e+f+g)hk+c(d+h)k)s^2+cd(e+f+g)hks^4)+s^2(c+e+f+g+k+n+((e+f+g)hk \\ & +((e+f+g)h+(e+f+g+k)m)n+c(hk+(h+m)n+d(e+f+g+k+n)))s^2 \\ & +(cd(e+f+g)hk+(e+f+g)hkmn+c(d(e+f+g)h+hkm+d(e+f+g+k)m)n)s^4 \\ & +cd(e+f+g)hkmns^6)z \end{aligned} \tag{16}$$

According to the calculated insertion loss, the transmission zeros of the asymmetric resonator can be given as follows:

$$\text{Fz1} - \text{Asymetric Resonator} = \frac{1}{2\pi}\sqrt{\frac{M}{3N}+\frac{2^{\frac{1}{3}}\left(-M^2+3HN\right)}{3N\left(-2M^3+9HMN-27GN^2+\sqrt{4\left(-M^2+3HN\right)^3+\left(-2M^3+9HMN-27GN^2\right)^2}\right)^{\frac{1}{3}}}-\frac{\left(-2M^3+9HMN-27GN^2+\sqrt{4(-M^2+3HN)^3+(-2M^3+9HMN-27GN^2)^2}\right)^{1/3}}{32^{1/3}N}} \tag{17}$$

$$\text{Fz} - \text{Asymetric Resonator Resonator} = \frac{1}{2\pi}\sqrt{\frac{M}{3N}-\frac{\left(1+\sqrt{3}\right)\left(-M^2+3HN\right)}{32^{\frac{2}{3}}N\left(-2M^3+9HMN-27GN^2+\sqrt{4\left(-M^2+3HN\right)^3+\left(-2M^3+9HMN-27GN^2\right)^2}\right)^{\frac{1}{3}}}+\frac{\left(1-\sqrt{3}\right)\left(-2M^3+9HMN-27GN^2+\sqrt{4(-M^2+3HN)^3+(-2M^3+9HMN-27GN^2)^2}\right)^{1/3}}{62^{1/3}N}} \tag{18}$$

$$\mathrm{Fz3-Asymetric\ Resonator\ Resonator} = \frac{1}{2\pi}\sqrt{\frac{M}{3N}-\frac{\left(1-\sqrt{3}\right)\left(-M^2+3HN\right)}{32^{\frac{2}{3}}N\left(-2M^3+9HMN-27GN^2+\sqrt{4\left(-M^2+3HN\right)^3+\left(-2M^3+9HMN-27GN^2\right)^2}\right)^{\frac{1}{3}}}+\frac{(1+\sqrt{3})(-2M^3+9HMN-27GN^2+\sqrt{4(-M^2+3HN)^3+(-2M^3+9HMN-27GN^2)^2})^{1/3}}{62^{1/3}N}} \quad (19)$$

where

$$G(C3+C4+C5+CSP+C6+C7+C8) \quad (20)$$

$$\begin{aligned} H &= (C4L4C7+C5L4C7+(Csp+C6)L4C7+C4L4C8+C5L4C8+(Csp+C6)L4C8+C4L5C8 \\ &\quad +C5L5C8+L5(Csp+C6)C8+L5C7C8+C3L4C7+L4C3C8+L5C8C3+C4C3L3 \\ &\quad +C5C3L3+(Csp+C6)C3L3+C7C3L3+C8C3L3). \quad (21) \\ M &= (C4C3L3L4C7+C5C3L3L4C7+(Csp+C6)C3L3L4C7+C4L4C7L5C8+C5L4C7L5C8 \\ &\quad +(Csp+C6)L4C7L5C8+C4L3L4C8C3+C5L3L4C8C3+(Csp+C6)L3L4C8C3 \\ &\quad +L4C7L5C8C3+C4L5L3C8C3+C5L5L3C8C3+(Csp+C6)L5L3C8C3+L5C7L3C8C3). \quad (22) \\ N &= (C4C3L3L4C7L5C8+C5C3L3L4C7L5C8+(Csp+C6)C3L3L4C7L5C8). \quad (23) \end{aligned}$$

According to Equations (17)–(19), applying asymmetric coupled lines creates another transmission zero leading to improving the rejection band. To illustrate the effects of the asymmetry on the frequency response of the shown resonator in Fig. 3(a), several simulations versus Csp, L5, L6 and C7 are plotted in Figs. 4(a), 4(b), 4(c) and 4(d), respectively. As can be observed, by increasing the values of Csp, L5 and L6 from the shown minimum values to the determined maximum values, the second transition zero (FZ2) will move to lower frequencies causing a better rejection level from 1.8 GHz to 3 GHz. As observed from the simulation results depicted in Fig. 3(c), the cutoff frequency of the presented resonator with asymmetric coupled lines is located at 1.6 GHz. The stopband of this resonator suppresses spurious frequencies from 1.73 GHz to 8.61 GHz with corresponding attenuation level of −18.32 dB.

Table 1. The dimensions of the fabricated WPD (all in millimeter).

Lf	L1	L2	L3	L4	L5	L6	W1	W2	W3	W4	W5	S
0.5	6.7	1.9	6.8	3.3	5.4	5.9	0.2	0.1	0.2	1.2	0.1	0.2

Table 2. The values of lumped elements of the shown LC circuit in Fig. 3(b).

L1 (nH)	L2 (nH)	L3 (nH)	L4 (nH)	L5 (nH)	L6 (nH)	L7 (nH)	L8 (nH)	C1 (PF)	C2 (PF)
0.64	4.2	3.1	0.26	0.26	0.13	4.07	5.4	0.02	0.32
C3 (PF)	C4 (PF)	C5 (PF)	C6 (PF)	C7 (PF)	C8 (PF)	C9 (PF)	C10 (PF)	Csp (PF)	
0.29	0.78	0.085	1.91	1.01	0.25	0.49	0.126	1.29	

The insertion loss is approximately 0.63 dB from DC to 0.93 GHz which indicates an acceptable response in the passband. Clearly, this asymmetry has created a transmission zero (Fz2) between the primary transmission zeros (Fzp1 and Fzp2) of the shown resonator in Fig. 1(a). Moreover, Fzp2 is moved to higher frequencies leading to widening the suppression band. The dimensions of the depicted asymmetric hairpin resonator and the values of lumped elements are shown in Tables 1 and 2,

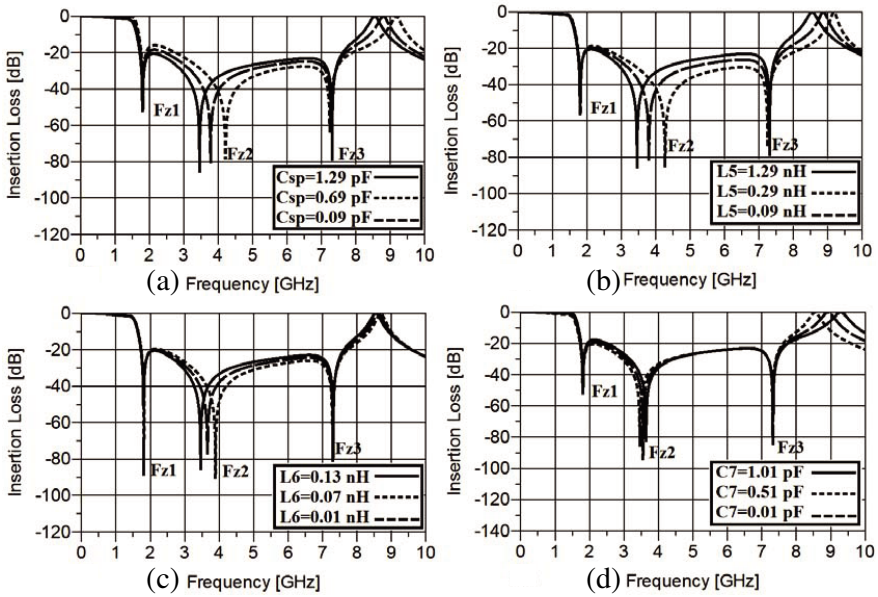

Figure 4. The behavior of the proposed asymmetric hairpin resonator against changing the values of (a) Csp, (b) $L5$, (c) $L6$, and (d) $C7$.

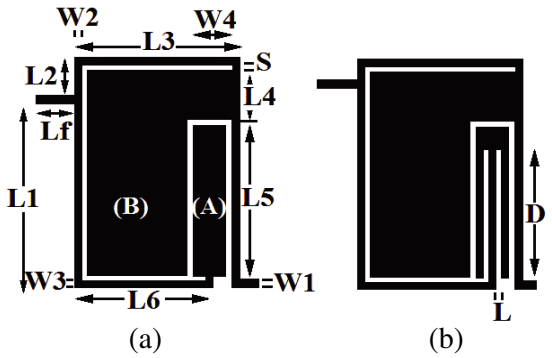

Figure 5. (a) The modified asymmetric hairpin resonator. (b) The modified asymmetric hairpin resonator with slots.

respectively. Moreover, the designed resonator creates three transmission zeros at 1.736 GHz, 3.33 GHz and 8.281 GHz with corresponding attenuation levels of −27.319, −45.316 and 39.014 dB, respectively, leading to a desired rejection band. In the next step, the other microstrip line determined by (A) is utilized to control the frequency response. To avoid increasing the occupied area, the dimensions of all microstrip lines of the resonator depicted in Fig. 3(a) will be kept constant.

As illustrated in Fig. 5, to improve the frequency response, a microstrip open-stub with slots is employed instead of the determined one by (A). The effects of increasing the length of the mentioned slots on the frequency response is illustrated in Fig. 6.

As can be observed from Fig. 6, by increasing the length of slot determined by (D) from zero to 4.5 mm with steps of 1.5, the first transition zero (FZ1) at 2.161 GHz will move to lower frequencies causing a sharper transition band. Since the operating frequency of the proposed designed is not affected markedly, this increase sharpens the transition band significantly. Furthermore, the third transmission zero moves toward lower frequencies, causing a better suppressing level without affecting the wideness of this region (see Fig. 6(a)). Finally, a microstrip lowpass filter with −3 dB opearating frequency of 1.69 GHz utilizing modified hairpin resonators with slots, which are placed symmetrically around (Y) axis is designed.

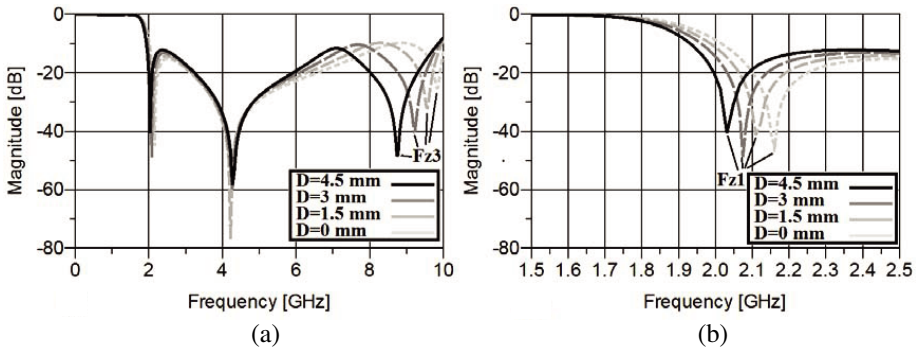

Figure 6. The behavior of the proposed hairpin resonator with slots against changing the value of D.

3. MEASUREMENT AND SIMULATION RESULTS

The configuration, photograph and frequency response of the proposed LPF are shown in Fig. 7. The presented LPF is designed, constructed and tested. The implemented LPF is fabricated on a substrate with the thickness of 0.508 mm, permittivity of 3.38 and loss tangent of 0.0021. The simulation and measurement results of the proposed LPF are depicted in Fig. 7(c). As can be observed, −3 dB cutoff frequency of the presented filter is located at 1.69 GHz. In the whole passband region the insertion loss is close to −0.2 dB, which illustrates a flat response.

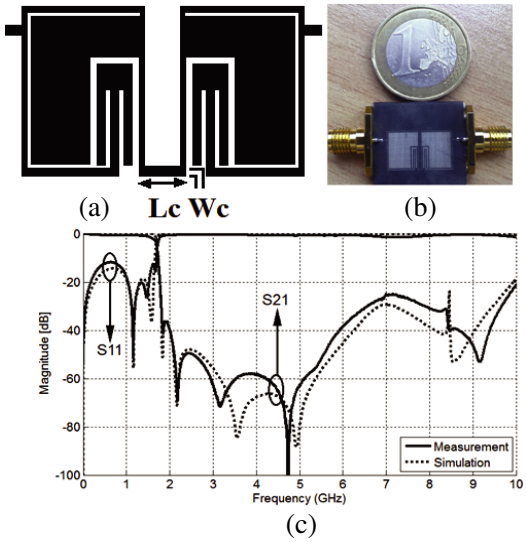

Figure 7. (a) The configuration of the proposed LPF. (b) A photograph of the proposed LPF. (c) The simulated and measured results of the proposed filter.

Furthermore, in this band the return loss is better than 14.3 dB. As seen, close to the operating frequency two transmission zeros (TZs) at 1837 and 2193 GHz with attenuation levels of −42.85 and −71.56 dB, respectively, exist leading to a steep roll-off rate. Thanks to these TZs, a sharp transition band about 0.14 GHz from 169 to 183 GHz with corresponding attenuation levels of −3 and −40 dB, respectively, is measured, which proves a desired skirt performance. The stopband region rejects spurious frequencies from 178 up to 10 GHz with corresponding rejection level of −20 dB. Table 1 shows the performance comparison of the other published works and the proposed LPF. In this table, the roll-off rate is defined as:

$$\zeta = \frac{\alpha_{\max} - \alpha_{\min}}{f_s - f_c} \,(\mathrm{dB/GHz}) \tag{24}$$

Table 3. Comparison between the performance of the proposed Lowpass Filter and previous works.

Ref.	Roll-Off Rate (ζ)	Relative Stopband Bandwidth (RSB)	Suppression Factor (SF)	Normalized circuit size (NCS)	Architecture Factor (AF)	Figure of merit (FOM)
[1]	30	1.25	1.5	0.080×0.080	1	8789
[2]	61.6	1.44	1	0.272×0.236	1	1386
[3]	62	1.72	3	0.310×0.240	1	4430
[4]	22	1.55	1.5	0.089×0.081	1	7095
[5]	37	1.65	1.5	0.111×0.091	1	9065
[6]	36.3	1.323	1.5	0.079×0.079	1	11543
[7]	37	1.15	2	0.280×0.076	1	3999
[8]	95	1.4	2	0.214×0.104	1	11951
[9]	130	0.933	2	0.227×0.089	2	6004
[10]	200	1.36	2	0.801×0.374	1	1815.9
[11]	250	1.82	2.2	0.219×0.072	1	63483
[12]	13	1.59	3.	0.0152		4832
[13]	185	1.66	2.	0.22×0.17		1618
This Work	**264**	**1.45**	**2**	**0.140×0.076**	**1**	**72032**

where $\alpha_{\max}$ is the -40 dB attenuation point, $\alpha_{\min}$ the -3 dB attenuation point, f_s the -40 dB stopband frequency, and f_c the -3 dB cutoff frequency. The relative stopband bandwidth (RSB) is given by:

$$\text{RSB} = \frac{\text{stopband bandwidth } h}{\text{stopband center frequency}} \tag{25}$$

The relative stopband bandwidth (RSB) of the lowpass filter is about 145%. The suppression factor (SF) is based on the stopband suppression. For example, if the stopband suppression is under 20 dB, then the SF is considered as 2. The normalized circuit size (NCS) is given by:

$$\text{NCS} = \frac{\text{physical size (length} \times \text{width)}}{{\lambda_g}^2} \tag{26}$$

where λ_g is the guided wavelength at 3 dB cutoff frequency. The architecture factor (AF) can be recognized as the complexity factor of the circuit, which is defined as 1 when the design is 2D and as 2 when the design is 3D. Finally, the figure-of-merit (FOM) is the overall index of the proposed filter, which is defined as:

$$\text{FOM} = \frac{RSB \times \zeta \times SF}{AF \times NCS} \tag{27}$$

4. CONCLUSION

A lowpass filter employing a pair of modified hairpin resonators which are placed symmetrically around (Y) axis is designed and fabricated. Based on the equivalent LC circuit of the proposed resonance cell, the equations of the insertion loss and return loss, and consequently the locations of transition zeros of the mentioned resonators are calculated. Moreover, according to the measurement results, a sharp roll-off rate, wide stopband, low insertion loss and return loss in the passband are achieved, verifying good in-band and out-band performances. Furthermore, this structure occupies a small area of $0.140\lambda_g \times 0.076\lambda_g$.

REFERENCES

1. Wei, X. B., P. Wang, M. Q. Liu, and Y. Shi, "Compact wide-stopband lowpass filter using stepped impedance hairpin resonator with radial stubs," *IEE Electron. Lett.*, Vol. 47, No. 15, 862–863, July 2011.
2. Wei, F., L. Chen, X.-W. Shi, Q.-L. Huang, and X.-H. Wang, "Compact lowpass filter with wide stop-band using coupled-line hairpin unit," *Electron. Lett.*, Vol. 46, No. 1, 88–90, 2010.
3. Ma, K. and K. S. Yeo, "New ultra-wide stopband low-pass filter using transformed radial stubs," *IEEE Trans. Microw. Theory. Tech.*, Vol. 59, No. 3, 604–611, March 2011.
4. Cui, H., J. Wang, and G. Zhang, "Design of microstrip lowpass filter with compact size and ultra-wide stopband," *IEE Electron. Lett.*, Vol. 48, No. 14, 856–857, July 2012.
5. Wang, J., H. Cui, and G. Zhang, "Design of compact microstrip lowpass filter with ultra-wide stopband," *IEE Electron. Lett.*, Vol. 48, No. 14, 854–856, July 2012.
6. Wang, J., L.-J. Xu, S. Zhao, Y.-X. Guo, and W. Wu, "Compact quasi-elliptic microstrip lowpass filter with wide stopband," *IEE Electron. Lett.*, Vol. 46, No. 20, 1384–1385, 2010.
7. Luo, S., L. Zhu, and S. Sun, "Stopband-expanded low-pass filters using microstrip coupled-line hairpin units," *IEEE Microw. Wireless Compon. Lett.*, Vol. 18, No. 8, 506–508, August 2008.
8. Velidi, V. K. and S. Sanyal, "Sharp roll-off lowpass filter with wide stopband using stub-loaded coupled-line hairpin unit," *IEEE Microw. Wireless Compon. Lett.*, Vol. 21, No. 6, 301–303, June 2011.
9. Mandal, M. K., P. Mondal, S. Sanyal, and A. Chakrabarty, "Low insertion-loss, sharp rejection and compact microstrip lowpass filter," *IEEE Microw. Wirel. Compon. Lett.*, Vol. 16, No. 11, 600–602, 2006.
10. Gomez-Garcia, R., M. A. Sanchez-Soriano, M. Sanchez Renedo, G. Torregrosa-Penalva, and E. Bronchalo, "Extended-stopband microstrip lowpass filter using rat-race directional couplers," *Electron. Lett.*, Vol. 49, No. 4, 272–274, 2013.
11. Abdipour, A., A. Abdipour, and S. Lotfi, "A lowpass filter with sharp roll-off and high relative stopband bandwidth using asymmetric high-low impedance patches," *Radio Engineering*, Vol. 24, No. 3, 712–716, 2015.
12. Nouritabar, A. R., A. Abdipour, and A. Abdipour, "A design of low-pass filter with wide stopband and sharp roll-off rate using series LC tanks resonator," *Applied Computational Electromagnetics Society (ACES) Journal*, Vol. 31, No. 11, 1343–1350, 2016.
13. Abdipour, A. and A. Abdipour, "Compact microstrip lowpass filter with an ultra-wide stopband and sharp transition band using T-shaped and polygon resonators," *Progress In Electromagnetics Research C*, Vol. 74, 51–61, 2017.
14. Abdipour, A., A. Abdipour, and F. Lorestani, "A compact microstrip lowpass filter with sharp roll-off rate and ultra-wide stopband employing coupled polygon patches," *Progress In Electromagnetics Research C*, Vol. 76, 171–183, 2017
15. Hong, J.-S. and M. J. Lancaster, *Microstrip Filters for RF/Microwave Applications*, John Wiley & Sons, Inc., 2001.
16. Du, Z., H. Yang., H. Zhang, and M. Zhu, "Compact LPF with sharp roll-off and wide stopband using coupling stepped impedance triangular resonator," *Progress In Electromagnetics Research Letters*, Vol. 44, 29–34, 2014.
17. Hsieh, L.-H. and K. Chang, "Compact lowpass filter using stepped impedance hairpin resonator," *Electron. Lett.*, Vol. 37, No. 14, 899–900, July 2001.